

Finite-temperature spin diffusion in the two-dimensional XY model

Erik Fitzner,¹ Byungjin Lee,² Junhyeok Hur,^{2,*} Minseok Kim,²
Benedikt Schneider,³ Jae-yoon Choi,^{2,†} and Björn Sbierski^{1,‡}

¹*Institut für Theoretische Physik, Universität Tübingen,
Auf der Morgenstelle 14, 72076 Tübingen, Germany*

²*Department of Physics, Korea Advanced Institute of Science and Technology,
Daehak 291, Daejeon, 34141, Republic of Korea*

³*Arnold Sommerfeld Center for Theoretical Physics, Center for NanoScience, and Munich Center for
Quantum Science and Technology, Ludwig-Maximilians-Universität München, 80333 Munich, Germany*

We present a combined theory-experiment study to quantify spin diffusion in the square lattice quantum spin-1/2 XY model at finite temperature. On the theory side, we leverage a recently developed dynamical high-temperature expansion method to faithfully capture the long spatiotemporal scales of the hydrodynamic regime. Experimental results are obtained from an optical lattice hard-core boson quantum simulator. The excellent agreement of spin diffusion constants marks a breakthrough in spin-transport beyond one dimension and for the quantitative validation of state-of-the-art quantum simulation platforms. We also provide theory predictions for future experiments on dynamic spin conductivity or anisotropy-induced integrability breaking.

Introduction.— Analog quantum simulation of many-body systems promises quantitative accuracy and the capability to obtain observables beyond the reach of numerical simulations on classical computers [1–4]. Fulfilling this promise requires careful navigation on the frontiers of both simulation approaches for cross-validation. One recurrent theme in this field considers the spatiotemporal diffusion process of a globally conserved quantity like particle number, charge or spin in a close-to-equilibrium situation. While the phenomenon of diffusion [5] is utterly classical in principle and can be subsumed in an experimentally accessible diffusion constant, its quantitative theoretical description in a chaotic many-body system demands an accurate solution of quantum dynamics governed by the Schrödinger equation for large time and length scales [6] which represents a formidable challenge.

The above aspects render the problem of diffusion an excellent case for cross-validation between analog quantum simulation and numerical algorithm development. In the following, we will focus on the important case of spin diffusion. Although much experimental effort has been directed to one-dimensional (1D) spin systems and the question under which conditions diffusive spin-dynamics is realized at all [7–16], quantitative study of spin diffusion in 2D, which occurs much more generically, has received much less attention. One outstanding experimental study by Nichols et al. [17] probed the equilibrium spin diffusion constant in a square-lattice Fermi-Hubbard model quantum simulator and mapped out its dependence on interaction strength. Remarkably, until now, seven years after the experiment, the obtained data could not be quantitatively reproduced theoretically [18]. This highlights the shortcomings of state-of-the-art numerical approaches to 2D quantum dynamics, and in particular the difficulty to account for the two vastly different model-specific spin transport time-scales, namely spin-exchange and particle hopping.

In this work we revisit the problem of equilibrium 2D spin diffusion theoretically and experimentally. For a fresh perspective, we focus on the simple and paradigmatic spin-1/2 XY model with nearest-neighbor exchange J on the square lattice which we realize in the hard-core limit of a large-scale Bose-Hubbard quantum simulator. On the theory side, the degree of difficulty is controlled by the single free parameter in the problem, the dimensionless inverse temperature J/T . We demonstrate a novel theoretical approach to 2D spin diffusion based on the recently introduced dynamic high-temperature expansion (Dyn-HTE [19, 20]) which outperforms existing state-of-the-art techniques in terms of temperature range and accuracy. On the experimental side, we obtain the spin diffusion constant from the late-

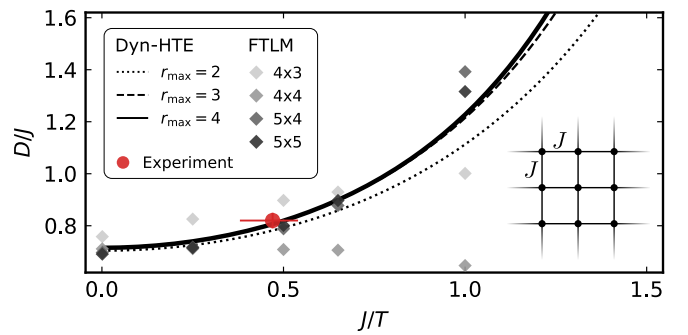


FIG. 1. Temperature dependence of the spin diffusion constant D for the square lattice XY model, see inset. Theoretical results from Dyn-HTE (lines) are compared to FTLM (diamonds, on $L_x \times L_y$ lattice), the latter method is severely restricted by finite size effects for $T \lesssim J$ where Dyn-HTE converges well in the number of included frequency moments r_{max} . The experimentally determined D (red dot) is significantly different from the theoretical $T = \infty$ prediction but is in excellent agreement with the prediction at finite J/T obtained by independent correlation-based thermometry.

time decay dynamics of a domain wall state. By invoking independent correlation-based thermometry, we achieve excellent agreement between the measured spin diffusion constant and the theoretical prediction, see Fig. 1. Our result thus presents an important milestone in the quantitative validation of analog 2D quantum simulation on the basis of quantum dynamics, highlights the importance of careful thermometry and enables various extensions to more complex observables or models. As an example for the latter, we theoretically study spin diffusion under the influence of controlled integrability breaking [21, 22] through lattice anisotropy.

XY model and spin diffusion.— We consider a square lattice of localized spin-1/2 with unit spacing and nearest-neighbor coupling of in-plane spin components,

$$H = \sum_{\mathbf{r}} J_x S_{\mathbf{r}}^+ S_{\mathbf{r}+\hat{x}}^- + J_y S_{\mathbf{r}}^+ S_{\mathbf{r}+\hat{y}}^- + \text{h.c.} \quad (1)$$

Here $S_{\mathbf{r}}^{\pm} = (S_{\mathbf{r}}^x \pm i S_{\mathbf{r}}^y)/\sqrt{2}$ with $S_{\mathbf{r}}^{x,y,z} = \sigma_{\mathbf{r}}^{x,y,z}/2$ spin operators at site \mathbf{r} expressed via Pauli matrices $\sigma_{\mathbf{r}}^{x,y,z}$ and $J_{x,y}$ denote potentially anisotropic coupling strengths (we start with the isotropic case $J_x = J_y \equiv J$ and set $\hbar = 1 = k_B$). The model exhibits a U(1) spin rotation symmetry about the spin- z axis so that the total magnetization $S^z = \sum_{\mathbf{r}} S_{\mathbf{r}}^z$ is conserved. The continuity equation on the lattice reads

$$\partial_t S_{\mathbf{r}}^z = -\nabla \cdot (j_{\mathbf{r}}^{(x)}, j_{\mathbf{r}}^{(y)}) \equiv j_{\mathbf{r}-\hat{x}/2}^{(x)} - j_{\mathbf{r}+\hat{x}/2}^{(x)} + j_{\mathbf{r}-\hat{y}/2}^{(y)} - j_{\mathbf{r}+\hat{y}/2}^{(y)}, \quad (2)$$

where spin(- z) bond currents follow from the equation of motion $\partial_t S_{\mathbf{r}}^z = i[H, S_{\mathbf{r}}^z]$, e.g. in x -direction $j_{\mathbf{r}}^{(x)} = j_{\mathbf{r}+\hat{x}/2}^{(x)} + j_{\mathbf{r}-\hat{x}/2}^{(x)}$ with the current between sites \mathbf{r} and $\mathbf{r} + \hat{x}$,

$$j_{\mathbf{r}+\hat{x}/2}^{(x)} = -i J_x (S_{\mathbf{r}}^+ S_{\mathbf{r}+\hat{x}}^- - S_{\mathbf{r}}^- S_{\mathbf{r}+\hat{x}}^+). \quad (3)$$

In other words, although spins are fixed in space, their mutual interaction leads to the spreading of z -magnetization throughout the system [7, 10, 23, 24]. In a (close-to) equilibrium state at temperature T , Fick's law governs the hydrodynamic relation between (weak) magnetization gradients and currents,

$$j_{\mathbf{r}}^{(x)} = -D \partial_x \langle S_{\mathbf{r}}^z \rangle, \quad (4)$$

with D the spin diffusion constant [10, 17, 24, 25]. This equation forms the basis for the experimental determination of D below. Here and in the following, we assume spin transport in x -direction and an infinite lattice. Note that D does not depend on the sign of J due to the bipartite nature of the lattice considered [26].

Theoretical approach via Dyn-HTE.— From a theory perspective the spin diffusion constant is best calculated using the linear-response framework [6]. For this it is required to drive the spin current not by a magnetization gradient but instead by a gradient of a Zeeman field

$h_{\mathbf{r}}^z S_{\mathbf{r}}^z$. The latter can be considered a perturbation to the Hamiltonian and thus fits into the framework of the Kubo formula [10, 24]. The so-obtained dissipative part of the response function is known as spin conductivity,

$$\sigma(\mathbf{k}, \omega) = \frac{1 - e^{-\omega/T}}{2\omega} \int_{-\infty}^{\infty} dt \sum_{\mathbf{r}} e^{i\omega t - i\mathbf{k} \cdot \mathbf{r}} \langle j_{\mathbf{r}}^{(x)}(t) j_{\mathbf{0}}^{(x)} \rangle. \quad (5)$$

This expression used the continuity equation (2), the fluctuation-dissipation theorem, and involves the time-evolved current operator $j_{\mathbf{r}}^{(x)}(t)$ in the Heisenberg picture [6]. Its correlator is evaluated in thermal equilibrium without any gradients, $\langle \dots \rangle = \text{tr}[\dots e^{-H/T}] / \text{tr} e^{-H/T}$. Finally, $\sigma(\mathbf{k}, \omega)$ relates to D via the Einstein relation [10],

$$D \cdot \chi = \lim_{\omega \rightarrow 0} \lim_{k \rightarrow 0} \sigma(\mathbf{k}, \omega). \quad (6)$$

Here and in the following $\mathbf{k} \equiv (k, 0)$ is understood, χ is the static zz -spin susceptibility and the limits select the hydrodynamic regime.

While Eqns. (5) and (6) provide a formally exact route to calculate D , its practical evaluation is challenging, as the hydrodynamic limit requires access to the current correlator for sufficiently long time scales and system sizes. At infinite temperature, this problem is addressed by established approaches such as the recursion method [27–29] or, more recently, spin fRG [30]. At finite T , however, the situation is less well controlled. Here, the finite- T Lanczos method (FTLM), based on quantum typicality [31, 32] and Lanczos recursion [33, 34] was used [24, 35, 36]. Our implementation of FTLM shows that its main restriction is the slow convergence of D with system size $L_x \times L_y$ (restricted to ~ 25 sites), see diamond markers in Fig. 1. We conclude that FTLM is only suitable for high temperatures $T \gtrsim J$.

We therefore apply the recently developed Dyn-HTE method [19, 20]. It operates in the thermodynamic limit and computes high-order HTEs for frequency moments of the dynamical structure factor (DSF),

$$S(\mathbf{k}, \omega) = \int_{-\infty}^{+\infty} \frac{dt}{2\pi} \sum_{\mathbf{r}} e^{i\omega t - i\mathbf{k} \cdot \mathbf{r}} \langle S_{\mathbf{r}}^z(t) S_{\mathbf{0}}^z \rangle. \quad (7)$$

The DSF can then be faithfully reconstructed from its resummed frequency moments by standard methods [19, 37]. This works down to moderately low temperatures $T \simeq J/4$. Here we have extended Dyn-HTE to the spin-1/2 XY model and to order 14 in J/T , see also Ref. 38 for a thermometry application in a Kagome Rydberg array.

We use the Fourier-transformed continuity equation (2) to connect DSF and spin conductivity [24],

$$\sigma(\mathbf{k}, \omega) = \omega(1 - e^{-\omega/T}) \pi S(\mathbf{k}, \omega) / k^2, \quad (8)$$

and obtain the HTEs for the frequency moments of $\lim_{k \rightarrow 0} \sigma(\mathbf{k}, \omega) \equiv \sigma(\omega)$ by taking advantage of Dyn-HTE's

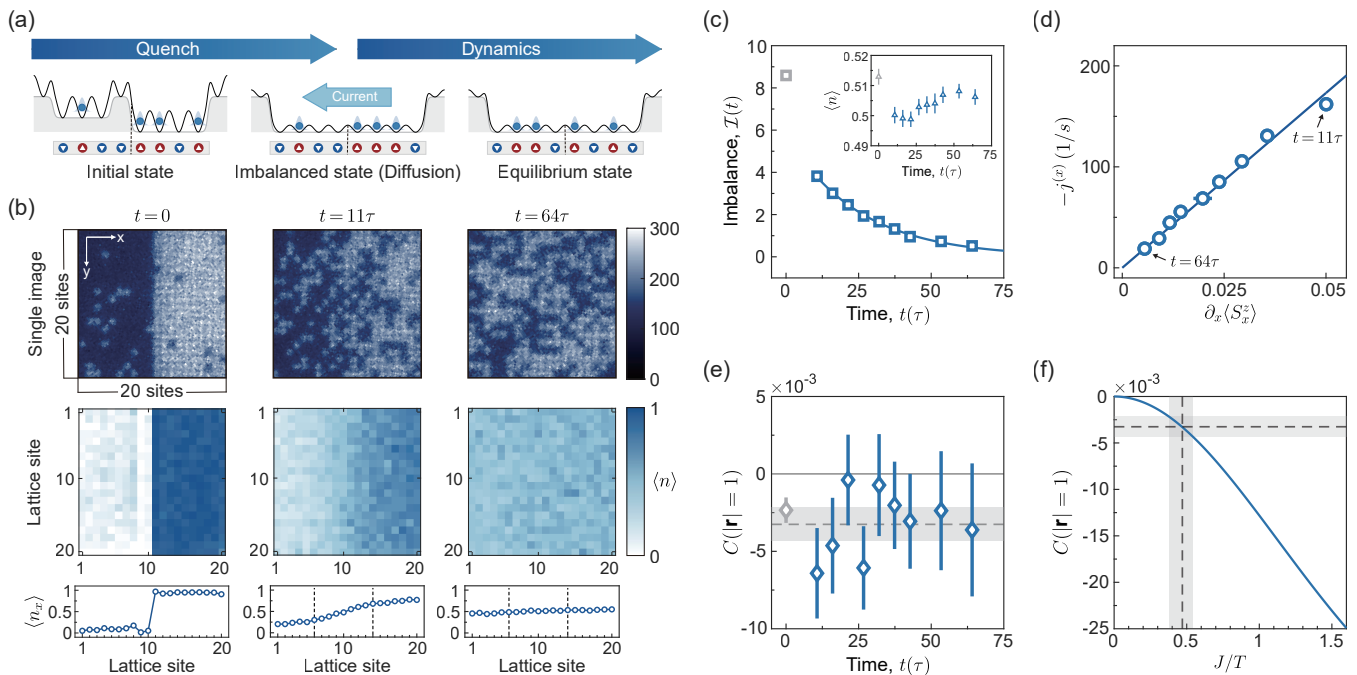


FIG. 2. (a) Illustration of the spin diffusion experiment using hard-core bosons. A wall potential with height $44t_{\text{BH}}$ is generated using a digital micromirror device (DMD). The total atom number is controlled by adjusting the offset potential in the left domain of the initial state through modification of the projected DMD pattern. (b) Time evolution of the system. The region of interest (ROI) for spin diffusion is 20×20 . Raw fluorescence images with a photoncount color scale (top), averaged 2D densities (middle), and density profiles $\langle n_x \rangle$ averaged along the y -axis (bottom). The spin gradient is obtained from a linear fit (not shown) to $\langle n_x \rangle$ over the central 9 sites between the dashed lines. (c) Time evolution of the density imbalance. The solid line shows an exponential fit with no time or vertical offsets, from which the spin current $j^{(x)}$ is obtained by differentiation. The initial time (gray point) is excluded from the fit. Error bars represent the standard error of the mean (SEM) and are smaller than the marker size. (Inset) Time evolution of atom density within the ROI. Atom density is conserved within $\langle n \rangle = [0.495, 0.515]$ during the dynamics. (d) Spin current as a function of the spin gradient $\partial_x \langle S_x^z \rangle$ at the center $x = 10$. The solid line represents a linear fit used to extract the spin diffusion constant D . Vertical errorbars represent the propagated 1σ uncertainty of the derivative of the exponential fit in (c), while horizontal errorbars represent the 1σ uncertainty from the linear fit to the spin gradient. Each data point in (b)–(d) is obtained from ~ 70 realizations. (e) Time evolution of the nearest-neighbor density correlator $C(\mathbf{r}) = \langle (n_{\mathbf{r}} - \langle n_{\mathbf{r}} \rangle)(n_{\mathbf{0}} - \langle n_{\mathbf{0}} \rangle) \rangle$ with $|\mathbf{r}| = 1$ averaged over the central 10×10 sites. The same data as in (b)–(d) are used, with density post-selection $\langle n \rangle = [0.475, 0.525]$ within the reduced ROI. The dashed line represents the mean correlation value during the dynamics, and the gray shaded region indicates the propagated SEM, $S = \sqrt{\sum_{i=1}^N s_i^2 / N}$ with $N = 9$. About 30 realizations are used for each point after post-selection. (f) Thermometry from nearest-neighbor correlation. The solid line shows the Dyn-HTE theory prediction. The horizontal dashed line and shaded region indicate the mean correlation value and its SEM from (e), while the vertical dashed line and shaded region indicate the extracted J/T and its uncertainty.

real-space formulation, see End Matter for details. Using similar resummation and reconstruction techniques as for the DSF [19], we access the limit $\omega \rightarrow 0$ and obtain $D(T)$ from Eq. (6) where we use a standard HTE for χ . Our results are shown in Fig. 1 and we explicitly demonstrate convergence with respect to the number of (even) frequency moments, $r_{\text{max}} = 2, 3, 4$ (various line styles) down to $T/J \simeq 2/3$ thereby outperforming FTLM.

Experiment.— Using a quantum simulator consisting of ultracold bosonic ^7Li atoms in an optical square lattice, we simulate the 2D isotropic Bose–Hubbard model,

$$H_{\text{BH}} = -\sum_{\mathbf{r}} t_{\text{BH}} (b_{\mathbf{r}}^\dagger b_{\mathbf{r}+\hat{x}} + b_{\mathbf{r}}^\dagger b_{\mathbf{r}+\hat{y}} + \text{h.c.}) + \frac{U}{2} \sum_{\mathbf{r}} n_{\mathbf{r}} (n_{\mathbf{r}} - 1). \quad (9)$$

Here, $b_{\mathbf{r}}$ ($b_{\mathbf{r}}^\dagger$) is the bosonic annihilation (creation) operator at site \mathbf{r} , t_{BH} is the nearest-neighbor tunneling amplitude, and U is the on-site interaction energy. In the hard-core regime, $t_{\text{BH}} \ll U$, H_{BH} maps onto the spin-1/2 XY model (1), with the mapping [11]

$$b_{\mathbf{r}}^\dagger = S_{\mathbf{r}}^x + i S_{\mathbf{r}}^y, \quad n_{\mathbf{r}} = b_{\mathbf{r}}^\dagger b_{\mathbf{r}} = S_{\mathbf{r}}^z - 1/2, \quad t_{\text{BH}} = -J/2. \quad (10)$$

The experiment begins by preparing a domain-wall state on an optical lattice with lattice spacing $a = 752 \text{ nm}$ [39] as shown in Fig. 2(a). A digital micromirror device (DMD) allows to generate arbitrary potentials and to tune the atom number in the left domain to satisfy the condition $\langle n \rangle \sim 0.5$ while avoiding doublons in the right domain. Starting from the initial state in Fig. 2(b) ($t = 0$), we rapidly switch the DMD potential

from domain-wall to a box (22×22 sites) and reduce the lattice depth to initiate the dynamics. During the evolution, the Bose-Hubbard parameters (see End Matter) are $t_{\text{BH}} = h \times 338(9)$ Hz and $U/t_{\text{BH}} = 30.2(8)$, under which the atom number is conserved within a 20×20 region of interest (ROI), see inset of Fig. 2(c). The ROI is chosen to minimize boundary effects of the box potential arising from the DMD point spread function [40, 41].

To determine the spin diffusion constant using Fick's law in Eq. (4), we measure the spin/density-current and -gradient at the center ($x = 10$). As shown in previous work [17], the spin current can be obtained from the time derivative of the density imbalance $\mathcal{I}(t) = \langle \sum_{x>10} n_x(t) - \sum_{x\leq 10} n_x(t) \rangle$, see Eq. (10). Here, $n_x(t)$ denotes the density averaged over the vertical y direction at time t . The tunneling time $\tau = \hbar/t_{\text{BH}} = 0.47(1)$ ms is shorter than the lattice quench duration of about 2τ , which is chosen to suppress band excitation [42]. For times beyond 11τ , the time evolution of the imbalance in Fig. 2(c) fits well to an exponential function with no offset. The current at the center of the box is obtained from the time derivative of the fitted imbalance curve as $-j^{(x)} = -(1/2)(d\mathcal{I}/dt)$. The spin/density gradient $\partial_x \langle S_x^z \rangle = \partial_x \langle n_x \rangle$ is extracted from a linear fit to $\langle n_x \rangle$ over the central 9 sites, with the fitting range indicated in the bottom panels of Fig. 2(b). The measured spin current $-j^{(x)}$ and the spin gradient $\partial_x \langle S_x^z \rangle$ fulfill a linear relation as predicted by Fick's law (4), see Fig. 2(d). A linear fit yields the diffusion constant $D = 0.82(3)J$, the uncertainty denotes the 1σ fitting error and we set $\hbar = 1$.

To determine the temperature of the close-to equilibrium state realized during the late-time domain wall melting dynamics, we measure the nearest-neighbor equal-time density correlator $C(\mathbf{r}) = \langle (n_{\mathbf{r}} - \langle n_{\mathbf{r}} \rangle)(n_{\mathbf{0}} - \langle n_{\mathbf{0}} \rangle) \rangle$ [43] with $|\mathbf{r}| = 1$, as shown in Fig. 2(e). We average the correlator over the same time interval as used for the diffusion measurement and compare to the corresponding (Dyn-)HTE prediction of $\langle S_x^z S_{\mathbf{0}}^z \rangle$ shown in Fig. 2(f) [44]. We obtain $J/T = 0.47_{-0.09}^{+0.07}$ and conclude that the experimental data point for $D(T)$ shown in Fig. 1 is in excellent agreement to the theory prediction.

Integrability breaking by anisotropy.— We finally generalize our theoretical considerations to the anisotropic case, i.e. Hamiltonian (1) with $J_x \neq J_y$. We keep x as the transport direction. Such anisotropy can be straightforwardly realized in optical lattice quantum simulators by independently tuning the laser intensities that define the optical lattice [40]. In the limit $J_y/J_x \rightarrow 0$, the system reduces to decoupled chains, which are integrable and show anomalous non-diffusive transport $\sigma(\omega) \propto \delta(\omega)$ [45]. By continuously tuning the ratio J_y/J_x we can therefore perform a controlled integrability breaking and monitor the crossover in spin transport. Our Dyn-HTE results for the diffusion constant are shown in Fig. 3 for various J_x/T , where we find $D/J_x \propto (J_y/J_x)^{-2}$ in the limit of

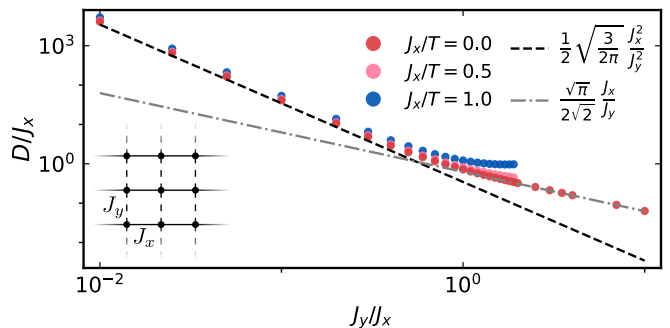


FIG. 3. Scaling of spin diffusion constant $D(T)$ with lattice anisotropy J_y/J_x (inset). In the limit $J_y/J_x \ll 1$, the diffusion constant follows a $D/J_x \propto (J_y/J_x)^{-2}$ scaling for all temperatures investigated. For $J_y/J_x \gtrsim 1$ and $J_x/T = 0$, a crossover to $D \propto (J_y/J_x)^{-1}$ is observed. Dashed/dash-dotted lines indicate analytical estimates based on Gaussian approximations, see End Matter for details.

weakly coupled chains $J_y/J_x \ll 1$, in agreement with Fermi's golden rule arguments [21, 22]. For $J_y/J_x \gtrsim 1$ and $T \rightarrow \infty$ we find a crossover to $D/J_x \propto (J_y/J_x)^{-1}$. Similar scalings have been reported for a ladder geometry [23]. For $D(T \rightarrow \infty)$ we derive simple but surprisingly accurate analytical expressions based on two complementary Gaussian approximations (dashed/dash-dotted lines and formulae in legend), see End Matter for details.

Note that similar integrability breaking in an XY-chain was recently studied experimentally [16] using Rydberg atoms with dipolar interaction. However, in this setup, the ratio of nearest- and integrability-breaking next-nearest-neighbor interaction ($J_2/J_1 = 1/8$) cannot be tuned. While late-time diffusive dynamics following a domain-wall quench was clearly observed, no quantitative determination of the diffusion constant was attempted.

Conclusion and outlook.— Interacting lattice spins are among the most simple and paradigmatic quantum many-body systems. Hence, diffusion of conserved magnetization is an elementary quantum-dynamic phenomenon in close-to equilibrium hydrodynamics. Despite this conceptual simplicity, to our knowledge no quantitative agreement between experimentally measured spin diffusion constants D and theoretical predictions have been achieved so far beyond 1D. Historically, in the field of solid-state quantum magnetism, this relates to challenges in driving and measuring spin currents over sufficient time and length scales. One rare example for such an experiment is Ref. 46, but the obtained value for D has still not been understood theoretically.

With the advancement of quantum simulation of spin models, the study of spin diffusion is rising to prominence again. Our work reports on the first match of a 2D spin diffusion constant between experiment and theory. This establishes a novel way for validation of quantum simulators. Moreover, the small error on the experimental value for D renders it incompatible with the theoretical

estimate at $T = \infty$ (c.f. Fig. 1) which highlights the need for careful thermometry and faithful inclusion of temperature on the theory side. This requires to go beyond simple methods that can only handle the large- T regime. We have tackled this challenge by demonstrating that the recently developed Dyn-HTE method provides a powerful and quantitatively reliable approach to equilibrium spin diffusion down to moderately low T/J . For other applications, note that Dyn-HTE is readily applicable for arbitrary lattice geometries and also in 3D.

Future work on the theory side could generalize Dyn-HTE to the Fermi-Hubbard model and finally provide a quantitative understanding of the spin diffusion measurement by Nichols et al. [17]. On the experimental side, numerous opportunities await, even for the XY model. First of all, the T -dependence of D could be resolved over a finite temperature range by controlled variation of entropy in the initial state. Second, using an anisotropic optical lattice, quantitative predictions on integrability breaking from Fig. 3 (and crossover time-scales to diffusive transport) could be investigated experimentally. Another worthwhile experiment could measure frequency (or momentum) dependent spin conductivity [47], for Dyn-HTE predictions on $\sigma(\omega)$ see End Matter. Finally, it would be interesting to leverage the flexibility of Rydberg-atom tweezer arrays [4, 16, 48] to quantitatively study spin diffusion in other lattice geometries and under the influence of the native long-range (dipolar XY) exchange interactions if limitations on experimental time-scales permit.

Data availability. — The data and code that support the findings of this work are openly available [49].

Acknowledgements. — We thank Peter Kopietz and Christian Groß for useful discussions. We acknowledge computational support by the state of Baden-Württemberg through bwHPC and the German Research Foundation (DFG) through Grant No. INST 40/575-1 FUGG (JUSTUS 2 cluster). We acknowledge funding from the Deutsche Forschungsgemeinschaft (DFG, German Research Foundation) through the Research Unit FOR 5413 (project N2), Grant No. 465199066, and National Research Foundation of Korea (NRF) Grant under Project No. RS-2023-NR119928, RS-2023-00256050, RS-2025-02220735, and RS-2026-25469704.

* Current address: Institut für Physik, Universität Tübingen, Auf der Morgenstelle 14, 72076 Tübingen, Germany

† jae-yoon.choi@kaist.ac.kr

‡ bjoern.sbierski@uni-tuebingen.de

- [1] E. Altman, K. R. Brown, G. Carleo, L. D. Carr, E. Demler, C. Chin, B. DeMarco, S. E. Economou, M. A. Eriksson, K.-M. C. Fu, M. Greiner, K. R. Hazzard, R. G. Hulet, A. J. Kollár, B. L. Lev, M. D. Lukin, R. Ma, X. Mi, S. Misra, C. Monroe, K. Murch, Z. Nazario, K.-K. Ni, A. C. Potter, P. Roushan, M. Saffman, M. Schleier-Smith, I. Siddiqi, R. Simmonds, M. Singh, I. Spielman, K. Temme, D. S. Weiss, J. Vučković, V. Vuletić, J. Ye, and M. Zwierlein, Quantum simulators: Architectures and opportunities, *PRX Quantum* **2**, 017003 (2021).
- [2] I. Bloch, J. Dalibard, and S. Nascimbène, Quantum simulations with ultracold quantum gases, *Nature Physics* **8**, 267 (2012).
- [3] I. M. Georgescu, S. Ashhab, and F. Nori, Quantum simulation, *Reviews of Modern Physics* **86**, 153 (2014).
- [4] T. Grass, D. Bercioux, U. Bhattacharya, M. Lewenstein, H. S. Nguyen, and C. Weitenberg, Colloquium: Synthetic quantum matter in nonstandard geometries, *Rev. Mod. Phys.* **97**, 011001 (2025).
- [5] L. P. Kadanoff, *Statistical Physics: Statics, Dynamics and Renormalization* (World Scientific, 2000).
- [6] H. Bruus and K. Flensberg, *Many-Body Quantum Theory in Condensed Matter Physics: An Introduction*, Oxford Graduate Texts (Oxford University Press, Oxford, New York, 2004).
- [7] X. Zotos, F. Naef, and P. Prelovsek, Transport and conservation laws, *Phys. Rev. B* **55**, 11029 (1997).
- [8] M. Žnidarič, Spin transport in a one-dimensional anisotropic heisenberg model, *Phys. Rev. Lett.* **106**, 220601 (2011).
- [9] R. Steinigeweg and W. Brenig, Spin transport in the XXZ chain at finite temperature and momentum, *Phys. Rev. Lett.* **107**, 250602 (2011).
- [10] B. Bertini, F. Heidrich-Meisner, C. Karrasch, T. Prosen, R. Steinigeweg, and M. Žnidarič, Finite-temperature transport in one-dimensional quantum lattice models, *Rev. Mod. Phys.* **93**, 025003 (2021).
- [11] J. P. Ronzheimer, M. Schreiber, S. Braun, S. S. Hodgman, S. Langer, I. P. McCulloch, F. Heidrich-Meisner, I. Bloch, and U. Schneider, Expansion dynamics of interacting bosons in homogeneous lattices in one and two dimensions, *Phys. Rev. Lett.* **110**, 205301 (2013).
- [12] H. Maeter, A. A. Zvyagin, H. Luetkens, G. Pasqua, Z. Shermadini, R. Saint-Martin, A. Revcolevschi, C. Hess, B. Büchner, and H.-H. Klauss, Low temperature ballistic spin transport in the S=1/2 antiferromagnetic heisenberg chain compound SrCuO₂, *J. Phys.: Condens. Matter* **25**, 365601 (2013).
- [13] F. Xiao, J. S. Möller, T. Lancaster, R. C. Williams, F. L. Pratt, S. J. Blundell, D. Ceresoli, A. M. Barton, and J. L. Manson, Spin diffusion in the low-dimensional molecular quantum heisenberg antiferromagnet Cu(py₂z)(NO₃)₂ detected with implanted muons, *Phys. Rev. B* **91**, 144417 (2015).
- [14] U. Schneider, L. Hacker Müller, J. P. Ronzheimer, S. Will, S. Braun, T. Best, I. Bloch, E. Demler, S. Mandt, D. Rasch, and A. Rosch, Fermionic transport and out-of-equilibrium dynamics in a homogeneous hubbard model with ultracold atoms, *Nat. Phys.* **8**, 213 (2012).
- [15] D. Wei, A. Rubio-Abadal, B. Ye, F. Machado, J. Kemp, K. Srakaew, S. Hollerith, J. Rui, S. Gopalakrishnan, N. Y. Yao, I. Bloch, and J. Zeiher, Quantum gas microscopy of Kardar-Parisi-Zhang superdiffusion, *Science* **376**, 716 (2022).
- [16] C. Chen, L. Capizzi, A. Marché, G. Bornet, G. Emperauger, T. Lahaye, A. Browaeys, M. Fagotti, and L. Mazza, Observing weakly broken conservation laws in a dipolar rydberg quantum spin chain (2026), [arXiv:2602.02251](https://arxiv.org/abs/2602.02251).

- [17] M. A. Nichols, L. W. Cheuk, M. Okan, T. R. Hartke, E. Mendez, T. Senthil, E. Khatami, H. Zhang, and M. W. Zwierlein, Spin transport in a mott insulator of ultracold fermions, *Science* **363**, 383 (2019).
- [18] L. Pham and E. Khatami, Spin and Charge Conductivity in the Square Lattice Fermi-Hubbard Model (2026), [arXiv:2602.03771](https://arxiv.org/abs/2602.03771).
- [19] R. Burkard, B. Schneider, and B. Sbierski, Dynamic correlations of frustrated quantum spins from high-temperature expansion, *Phys. Rev. Lett.* **136**, 056501 (2026).
- [20] R. Burkard, B. Schneider, and B. Sbierski, High-temperature series expansion of the dynamic Matsubara spin correlator, *Phys. Rev. B* **113**, 075102 (2026).
- [21] P. Jung, R. W. Helmes, and A. Rosch, Transport in Almost Integrable Models: Perturbed Heisenberg Chains, *Phys. Rev. Lett.* **96**, 067202 (2006).
- [22] P. Jung and A. Rosch, Spin conductivity in almost integrable spin chains, *Phys. Rev. B* **76**, 245108 (2007).
- [23] R. Steinigeweg, F. Heidrich-Meisner, J. Gemmer, K. Michielsen, and H. De Raedt, Scaling of diffusion constants in the spin- $\frac{1}{2}$ XX ladder, *Phys. Rev. B* **90**, 094417 (2014).
- [24] Bonča, J. and Jaklič, J., Spin diffusion of the t-J model, *Phys. Rev. B* **51**, 16083 (1995).
- [25] J. F. Wienand, S. Karch, A. Impertro, C. Schweizer, E. McCulloch, R. Vasseur, S. Gopalakrishnan, M. Aidelsburger, and I. Bloch, Emergence of fluctuating hydrodynamics in chaotic quantum systems, *Nat. Phys.* **20**, 1732 (2024).
- [26] This follows from a π_z spin rotation on one sublattice which flips the sign of J but leaves the zz -DSF (7) and thus, by Eqns. (6) and (8), also D invariant.
- [27] D. G. McFadden and R. A. Tahir-Kheli, Space-Time Correlations in Anisotropic Heisenberg Paramagnets at Elevated Temperatures, *Phys. Rev. B* **1**, 3649 (1970).
- [28] T. Morita, Spin Diffusion in the Heisenberg Magnets at Infinite Temperature, *Phys. Rev. B* **6**, 3385 (1972).
- [29] J. Wang, M. H. Lamann, R. Steinigeweg, and J. Gemmer, Diffusion constants from the recursion method, *Phys. Rev. B* **110**, 104413 (2024).
- [30] D. Tarasevych and P. Kopietz, Dissipative spin dynamics in hot quantum paramagnets, *Phys. Rev. B* **104**, 024423 (2021).
- [31] A. Hams and H. De Raedt, Fast algorithm for finding the eigenvalue distribution of very large matrices, *Phys. Rev. E* **62**, 4365 (2000).
- [32] P. Reimann, Dynamical typicality of isolated many-body quantum systems, *Phys. Rev. E* **97**, 062129 (2018).
- [33] C. Lanczos, An iteration method for the solution of the eigenvalue problem of linear differential and integral operators, *J. Res. Natl. Bur. Stand. B* **45**, 255 (1950).
- [34] A. W. Sandvik, A. Avella, and F. Mancini, Computational Studies of Quantum Spin Systems, in *AIP Conference Proceedings* (AIP, 2010) p. 135–338.
- [35] J. Jaklič and P. Prelovšek, Lanczos method for the calculation of finite-temperature quantities in correlated systems, *Phys. Rev. B* **49**, 5065 (1994).
- [36] T. Shimokawa, S. Sabharwal, and N. Shannon, Can experimentally-accessible measures of entanglement distinguish quantum spin liquids from disorder-driven "random singlet" phases? (2025), [arXiv:2505.11874](https://arxiv.org/abs/2505.11874).
- [37] V. S. Viswanath and G. Müller, *The Recursion Method: Application to Many-Body Dynamics*, Vol. 23 (Springer Science+Business Media, 1994).
- [38] E. Fitzner, I. Lesanovsky, and B. Sbierski, Thermometry for a Kagome Lattice Dipolar Rydberg Simulator (2026), [arXiv:2604.22743](https://arxiv.org/abs/2604.22743).
- [39] K. Kwon, K. Kim, J. Hur, S. Huh, and J.-y. Choi, Site-resolved imaging of a bosonic mott insulator of ^7Li atoms, *Phys. Rev. A* **105**, 033323 (2022).
- [40] J. Hur, J. Li, B. Lee, K. Kwon, M. Kim, S. Hwang, S. Kim, Y. S. Yu, A. Chan, T. Wahl, and J.-y. Choi, Stability of many-body localization in two dimensions (2025), [arXiv:2508.20699](https://arxiv.org/abs/2508.20699).
- [41] K. Kwon, K. Fujimoto, J. Hur, B. Lee, S. Hwang, S. Kim, R. Hamazaki, Y. Kawaguchi, and J.-y. Choi, Universal family-vice scaling in quantum gases far from equilibrium (2026), [arxiv:2603.09060](https://arxiv.org/abs/2603.09060).
- [42] T. Gericke, F. Gerbier, A. Widera, S. Fölling, O. Mandel, and I. Bloch, Adiabatic loading of a bose-einstein condensate in a 3d optical lattice, *J. Mod. Opt.* **54**, 735 (2007).
- [43] M. Boll, T. A. Hilker, G. Salomon, A. Omran, J. Nespolo, L. Pollet, I. Bloch, and C. Gross, Spin- and density-resolved microscopy of antiferromagnetic correlations in Fermi-Hubbard chains, *Science* **353**, 1257 (2016).
- [44] Equal time correlators $\langle S_i^z S_0^z \rangle$ can be simply obtained from frequency sums of the Dyn-HTE for Matsubara correlators [20, 38].
- [45] M. A. Cazalilla, R. Citro, T. Giamarchi, E. Orignac, and M. Rigol, One dimensional bosons: From condensed matter systems to ultracold gases, *Rev. Mod. Phys.* **83**, 1405 (2011).
- [46] J. Labrujere, T. O. Klaassen, and N. J. Poulis, Spin dynamics in a 3D Heisenberg ferromagnet in the paramagnetic state II, *J. Phys. C: Solid State Phys.* **15**, 999 (1982).
- [47] R. Anderson, F. Wang, P. Xu, V. Venu, S. Trotzky, F. Chevy, and J. H. Thywissen, Conductivity Spectrum of Ultracold Atoms in an Optical Lattice, *Phys. Rev. Lett.* **122**, 153602 (2019).
- [48] C. Chen, G. Bornet, M. Bintz, G. Emperauger, L. Leclerc, V. S. Liu, P. Scholl, D. Barredo, J. Hauschild, S. Chatterjee, M. Schuler, A. M. Läuchli, M. P. Zaletel, T. Lahaye, N. Y. Yao, and A. Browaeys, Continuous symmetry breaking in a two-dimensional Rydberg array, *Nature* **616**, 691 (2023).
- [49] E. Fitzner, [Data and code: https://zenodo.org/records/20277955](https://zenodo.org/records/20277955) (2026).
- [50] J. Oitmaa, C. Hamer, and W. Zheng, *Series Expansion Methods for Strongly Interacting Lattice Models* (Cambridge University Press, Cambridge, 2006).
- [51] D. Mitra, P. T. Brown, E. Guardado-Sanchez, S. S. Kondov, T. Devakul, D. A. Huse, P. Schauß, and W. S. Bakr, Quantum gas microscopy of an attractive fermi-hubbard system, *Nat. Phys.* **14**, 173 (2018).
- [52] C. Chin, R. Grimm, P. Julienne, and E. Tiesinga, Feshbach resonances in ultracold gases, *Rev. Mod. Phys.* **82**, 1225 (2010).
- [53] J. Amato-Grill, N. Jepsen, I. Dimitrova, W. Lunden, and W. Ketterle, Interaction spectroscopy of a two-component mott insulator, *Phys. Rev. A* **99**, 033612 (2019).
- [54] T. Stöferle, H. Moritz, C. Schori, M. Köhl, and T. Esslinger, Transition from a strongly interacting 1d superfluid to a mott insulator, *Phys. Rev. Lett.* **92**, 130403 (2004).

END MATTER

Spin conductivity from Dyn-HTE.— As shown in Eq. (8), the spin conductivity $\sigma(\mathbf{k}, \omega)$ is directly related to the DSF $S(\mathbf{k}, \omega)$ which was the initial objective of Dyn-HTE [19, 20]. For technical reasons, the method computes the HTE of the even frequency moments $m_{\mathbf{k}, 2r}$ ($r = 0, 1, 2, \dots$) of the (even) relaxation function, $R_{\mathbf{k}}(w) = TA_{\mathbf{k}}(\omega)/(2\pi w)$, where $w = \omega/J_x$ and $A_{\mathbf{k}}(\omega) = (1 - e^{-\omega/T})2\pi S(\mathbf{k}, \omega)$ is the spectral function. Hence, the moments of $\lim_{k \rightarrow 0} \sigma(\mathbf{k}, \omega) \equiv \sigma(\omega)$ are

$$\langle w^{2(r-1)} \rangle \equiv \int_{-\infty}^{\infty} dw w^{2(r-1)} \sigma(\omega) = \pi \frac{J_x}{T} \lim_{k \rightarrow 0} \frac{m_{\mathbf{k}, 2r}}{k^2}. \quad (11)$$

In practice, the flexibility of Dyn-HTE rests on a real-space graph-embedding strategy of results pre-calculated for all possible lattice snippets (graphs) [20, 50]. This means that the moments are naturally available in real-space, $m_{\mathbf{r}\mathbf{r}', 2r}$. For translation invariant and inversion-symmetric systems, we set $\mathbf{r}' = \mathbf{0}$ as the reference site and the $k \rightarrow 0$ limit can be evaluated explicitly as

$$\begin{aligned} \lim_{k \rightarrow 0} \frac{m_{\mathbf{k}, 2r}}{k^2} &= \lim_{k \rightarrow 0} \frac{1}{k^2} \sum_{\mathbf{r}} \cos(\mathbf{k} \cdot \mathbf{r}) m_{\mathbf{r}\mathbf{0}, 2r} \\ &\stackrel{r \geq 0}{=} -\frac{1}{2} \sum_{\mathbf{r}} (r^x)^2 m_{\mathbf{r}\mathbf{0}, 2r}, \end{aligned} \quad (12)$$

where $\mathbf{r} = (r^x, r^y)$, $\mathbf{k} = (k, 0)$ and we used $\sum_{\mathbf{r}} m_{\mathbf{r}\mathbf{0}, 2r} = 0$ for $r > 0$ from the static nature of the uniform susceptibility. Following the standard Dyn-HTE analytic continuation via a continued-fraction representation [19], we obtain an estimate for $\sigma(\omega)$. Combined with Eq. (6), this yields the spin diffusion constant $D = \lim_{\omega \rightarrow 0} \sigma(\omega)/\chi$, where we again employ the Dyn-HTE framework to obtain a numerical value for the static uniform (zz -)spin susceptibility, $\chi = \sum_{\mathbf{r}} \langle S_{\mathbf{0}}^z S_{\mathbf{r}}^z \rangle / T$. In Fig. 4, we show $\sigma(\omega)/(J\chi)$ at infinite temperature (where $1/\chi = 4T$) for the isotropic square lattice, computed with increasing accuracy by including moments up to $r_{max} = 2, \dots, 7$. For $\omega \rightarrow 0$, we obtain a well-converged value

$$(D/J)_{T=\infty}^{\text{square lattice}} \approx 0.72, \quad (13)$$

in excellent agreement with Ref. 28. For the two-leg ladder, we find

$$(D/J)_{T=\infty}^{\text{ladder}} \approx 0.95, \quad (14)$$

also in very good agreement with previously reported values [23, 29], supporting the reliability of our method.

Finally, note that HTE of moments $m_{\mathbf{r}\mathbf{r}', 2r}$ are available up to order $(J_x/T)^{14-2r}$. For $T < \infty$, this means that the moment's expansion order decreases with increasing r and we cannot faithfully resum the too short series for $r_{max} = 5, 6, 7$. This explains the restriction to $r_{max} = 2, 3, 4$ in Fig. 1.

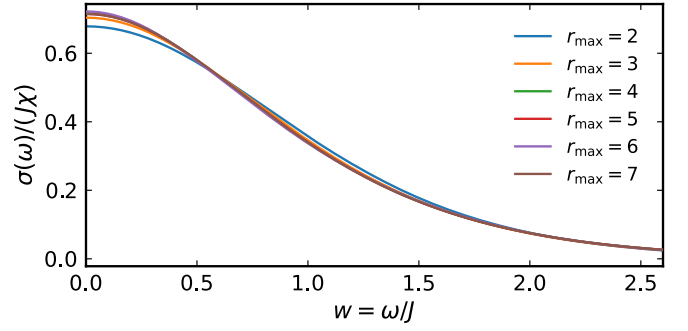


FIG. 4. Frequency-resolved spin conductivity $\sigma(\omega)$ at $T = \infty$ for the isotropic square lattice XY model, computed using an increasing number of moments r_{max} . The spin diffusion constant $D = \lim_{\omega \rightarrow 0} \sigma(\omega)/\chi$ is well-converged in r_{max} .

Gaussian approximation.— At infinite temperature and for simple models without multiple energy scales, it is often a good approximation to assume that $\sigma(\omega)$ is a Gaussian, see e.g. Ref. 24 and Fig. 4,

$$\sigma(\omega) = a e^{-b\omega^2}, \quad (15)$$

where $a, b \geq 0$ are parameters left to be determined. Within this approximation, the only two independent frequency moments are $\langle \omega^0 \rangle = a\sqrt{\pi/b}$ and $\langle \omega^2 \rangle = \frac{a}{2b}\sqrt{\pi/b}$. The Einstein relation (6) then yields

$$D_{\text{Gauss}} = \frac{a}{\chi} = \frac{1}{\chi\sqrt{2\pi}} \sqrt{\frac{\langle \omega^0 \rangle^3}{\langle \omega^2 \rangle}}. \quad (16)$$

At infinite temperature, these frequency moments can be evaluated straightforwardly:

$$\begin{aligned} \langle \omega^{2r} \rangle &\equiv \int_{-\infty}^{\infty} d\omega \omega^{2r} \sigma(\omega) \\ &= \frac{1}{2NT} \int_{-\infty}^{\infty} d\omega \omega^{2r} \int_{-\infty}^{\infty} dt e^{i\omega t} \langle j^{(x)}(t) j^{(x)}(0) \rangle \\ &= \frac{1}{2NT} \int_{-\infty}^{\infty} d\omega \int_{-\infty}^{\infty} dt \left\{ (i\partial_t)^{2r} e^{i\omega t} \right\} \langle j^{(x)}(t) j^{(x)}(0) \rangle \\ &= \frac{\pi}{NT} \left\langle \left\{ (i\partial_t)^{2r} j^{(x)}(t) \right\} j^{(x)}(0) \right\rangle_{|t=0} \\ &= \frac{\pi}{NT} \left\langle [\dots [j^{(x)}, H], H] \dots j^{(x)} \right\rangle, \end{aligned}$$

with a $2r$ -fold commutator and $j^{(x)} = \sum_{\mathbf{r}} j_{\mathbf{r}}^{(x)}$ the total (zero-momentum) spin current. This can be simplified as the product of two r -fold commutators [37],

$$\langle \omega^{2r} \rangle = \frac{\pi}{NT} (-1)^r \left\langle [\dots [j^{(x)}, H], \dots] \cdot [\dots [j^{(x)}, H], \dots] \right\rangle, \quad (17)$$

and we insert $j^{(x)}$ above Eq. (3) and H from Eq. (1) to

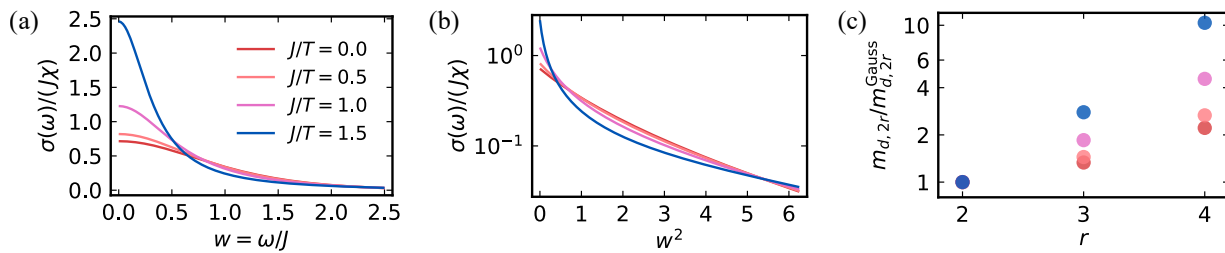


FIG. 5. Deviations of $\sigma(\omega)$ from Gaussian behavior in the isotropic square lattice XY model. (a) Frequency dependence for different temperatures J/T . (b) The same data plotted as a function of w^2 on a logarithmic scale, where a Gaussian appears linear. (c) Ratio of higher-order frequency moments to their Gaussian counterparts.

find after lengthy but straightforward algebra

$$\langle \omega^0 \rangle = \frac{\pi J_x^2}{8T}, \quad (18)$$

$$\langle \omega^2 \rangle = \frac{\pi J_x^2 J_y^2}{8T}, \quad (19)$$

$$\langle \omega^4 \rangle = \frac{3\pi J_x^4 J_y^2}{32T} + O(J_x^3 J_y^3) + O(J_x^2 J_y^4). \quad (20)$$

In the following, we use these moments to rationalize the anisotropy scaling of the diffusion constant at infinite temperature within the Gaussian approximation (see Fig. 3). We distinguish two cases, the close-to-integrable weakly coupled case $J_y \ll J_x$ and the opposite case $J_y \gtrsim J_x$ (which includes $J_y \gg J_x$). We start with the second case.

For $J_y \gtrsim J_x$ we expect ordinary diffusive transport and the Gaussian approximation (15) to be valid [24]. It then follows, with the pre-calculated moments (18)–(19) and $1/\chi = 4T$,

$$D = \frac{1}{\chi \sqrt{2\pi}} \sqrt{\frac{\langle \omega^0 \rangle^3}{\langle \omega^2 \rangle}} = \frac{\sqrt{\pi}}{2\sqrt{2}} \cdot \frac{J_x^2}{J_y} \simeq 0.63 \cdot \frac{J_x^2}{J_y}, \quad (21)$$

shown as dash-dotted line in Fig. 3 which matches Dyn-HTE at $J_x/T = 0$ within a few percent and explains the observed scaling.

For $J_y \ll J_x$ we follow the general strategy outlined in Ref. 21. We first consider the decoupled limit $J_y = 0$, where the XY chain is integrable and the total spin current is conserved, $[j^{(x)}, H] = 0$. As a consequence, the spin conductivity is purely ballistic,

$$\begin{aligned} \sigma(\omega)|_{J_y=0} &= \frac{1}{2NT} \int_{-\infty}^{\infty} dt e^{i\omega t} \langle j^{(x)}(t) j^{(x)}(0) \rangle \\ &= \delta(\omega) \frac{\pi J_x^2}{8T}. \end{aligned} \quad (22)$$

A weak transverse coupling $J_y \ll J_x$ breaks integrability and broadens the δ -peak. We model this by a Lorentzian of width $\Gamma(\omega) \propto J_y^2$ representing the scattering rate,

$$\sigma(\omega) = \frac{1}{T} \frac{\Gamma(\omega)}{(8\Gamma(\omega)/J_x^2)^2 + \omega^2}, \quad (23)$$

which reduces to Eq. (22) in the limit $\Gamma \rightarrow 0$. The diffusion constant then follows as

$$D = \frac{\lim_{\omega \rightarrow 0} \sigma(\omega)}{\chi} = \frac{J_x^4}{64 \chi \Gamma(0) T}. \quad (24)$$

For $\Gamma(\omega) \ll J_x^2$, the frequency moments of Eq. (23) can be approximated to leading order in J_y as

$$\langle \omega^{2r} \rangle \simeq \int_{-\infty}^{\infty} d\omega \omega^{2r-2} \Gamma(\omega)/T, \quad (r = 1, 2, \dots). \quad (25)$$

The moments (19) and (20) are sufficient to evaluate the parameters of a Gaussian ansatz for the scattering rate, $\Gamma(\omega) = a' e^{-b'\omega^2}$ [21]. We obtain

$$\Gamma(0) = a' = \frac{T}{\sqrt{2\pi}} \sqrt{\frac{\langle \omega^2 \rangle^3}{\langle \omega^4 \rangle}} = \frac{J_x J_y^2}{4} \sqrt{\frac{\pi}{6}}. \quad (26)$$

Inserting this into Eq. (24), we find

$$D = \frac{1}{2} \sqrt{\frac{3}{2\pi}} \frac{J_x^3}{J_y^2} \simeq 0.35 \cdot \frac{J_x^3}{J_y^2}, \quad (27)$$

in good agreement with the Dyn-HTE results, see dashed line in Fig. 3.

The last example around Eq. (23) implies that Dyn-HTE can access frequency dependence of $\sigma(\omega)$ beyond Gaussian lineshapes. In Fig. 5 we investigate this for the isotropic case and analyze $\sigma(\omega)$ at finite T , see panel (a). Panel (b) clearly reveals that deviations from a Gaussian shape are present even at $T = \infty$ and grow with J/T while panel (c) conveys the same message via the ratio of resummed frequency moments to their Gaussian counterparts.

Calibration of Bose-Hubbard parameters.— To implement the mapping from the Bose-Hubbard Hamiltonian to spin-1/2 XY Hamiltonian, it is necessary to ensure that the system is in the hard-core regime ($t_{\text{BH}} \ll U$). We set the lattice depth to $V_{\text{lat}} = 10.8E_r$, where $E_r = \hbar \times 12.6 \text{ kHz}$ is the recoil energy, in order to maximize the nearest-neighbor tunneling strength t_{BH} and minimize the effect of residual potential disorder ($\sim 80 \text{ Hz}$) in our system. We calibrate the tunneling strength

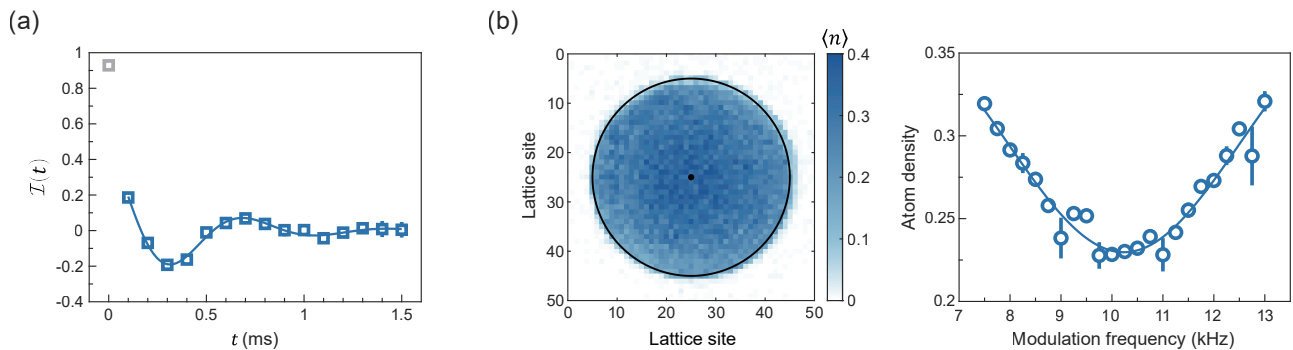


FIG. 6. (a) Calibration of the nearest-neighbor tunneling strength t_{BH} . The time evolution of the imbalance is fitted to a decaying Bessel function, $\mathcal{I}(t) = \mathcal{I}_0 e^{-\gamma(t-t_0)} \mathcal{J}_0(4t_{\text{BH}}(t-t_0))$, from which t_{BH} is extracted. Here, \mathcal{I}_0 is the imbalance amplitude, γ is the decay constant, and t_0 is a time offset accounting for the dynamics during the quench. The solid line shows that the fit to $\mathcal{I}(t)$, excluding the initial time (gray point). 8 realizations are used for each point. (b) Calibration of the on-site interaction U using modulation spectroscopy. A ring potential is applied to confine the atoms within the region of interest (ROI). (Left) Density distribution averaged over all measurements; the circle indicates the ROI and the dot marks the center. (Right) Atom density within the ROI as a function of the lattice modulation frequency. The solid line shows a Gaussian fit, and 10 data are used for each point. Error bars in (a) and (b) represent the standard error of the mean (SEM).

using a stripe initial state by fitting the time evolution of the imbalance to a decaying Bessel function, $\mathcal{I}(t) = \mathcal{I}_0 e^{-\gamma(t-t_0)} \mathcal{J}_0(4t_{\text{BH}}(t-t_0))$ [25, 40], as shown in Fig. 6(a). The experimentally obtained value is $t_{\text{BH}} = h \times 338(9)$ Hz, in good agreement with $t_{\text{BH}} = h \times 340$ Hz from a numerical calculation based on Wannier functions [51]. The initial point is excluded from the fit, since the shortest lattice quench duration without band excitation [42] is about 2τ , where $\tau = \hbar/t_{\text{BH}} = 0.47(1)$ ms is a tunneling time. As a result, the dynamics during the quench cannot be neglected, and we include a time offset t_0 in the decaying Bessel fit.

To realize the hard-core limit, we tune the magnetic

field to achieve $t_{\text{BH}} \ll U$ using a Feshbach resonance [52, 53]. The on-site interaction strength U is measured via modulation spectroscopy [54]. Owing to the short tunneling time, atoms escape from the region of interest during modulation. For this reason, a ring potential generated by a digital micromirror device (DMD) is used to confine the atoms, and the resulting density distribution is shown in Fig. 6(b). From the modulation spectroscopy, the on-site interaction is determined to be $U = h \times 10.2(0.02)$ kHz. The uncertainties of t_{BH} and U represent the 1σ fitting error. These results confirm the system is in the hard-core regime, $U/t_{\text{BH}} = 30.2(8)$.